# Supporting Information for

## *Operando* X-ray scattering study of segmented thermoelectric $Zn_4Sb_3$

Peter Skjøtt Thorup, Rasmus Stubkjær Christensen, Martin Roelsgaard, Bo Brummerstedt Iversen*

Center for integrated Materials Research, Department of Chemistry and iNANO, Aarhus University, DK-8000 Aarhus, Denmark

*E-mail: bo@chem.au.dk

## Table of Contents

1) Supplementary note 1 – Refinement Models ..... 2
2) Raw X-ray diffraction patterns for all samples ..... 4
3) Camera pictures of P- & S-250-10 samples ..... 8
4) Refined weight fraction of ZnSb for datasets 350-05, 350-10, and 250-05 ..... 9
5) Zoom of refined $Zn_4Sb_3$ weight fraction for P- & S-250-10 ..... 12
6) Residual $Zn_4Sb_3$ phase in the X-ray diffraction patterns ..... 13
7) Evolution of $R_{wp}$ for sample P-250-10 ..... 15
8) Decomposition rates for datasets 250-05, 350-05 and 350-10 ..... 16
9) Temperature gradient in P- & S-350-00 ..... 17
10) Refined occupancy of main site Zn1 for all samples ..... 18
11) Refined total Zn content for all samples ..... 20
12) Zn migration rates for datasets 250-05, 350-05, and 350-10 ..... 22
13) Zn peaks in raw diffraction patterns for S-250-10 ..... 23
14) Refined Zn weight fraction for sample P- & S-250-10 ..... 24
15) SEM images of sample S-350-10 ..... 25
16) SEM images of the Zn phase front ..... 26
17) SEM images of the ZnSb phase front ..... 27
18) SEM of second interface in sample S-250-10 ..... 28
19) References ..... 29

## 1) Supplementary note 1 – Refinement Models

The $Zn_4Sb_3$ phase used in all refinements were based on the three interstitial structure model by Snyder *et al*. (ICSD 168333).[1] The refined parameters were scale factor, unit cell parameters, atomic displacement factors (ADPs), and a linearly interpolated background. The ADPs were refined for Zn1, Sb1, Sb2, and the three interstitial sites Zn2,Zn3, and Zn4 were refined as equivalent. The peak profile was modelled using the instrumental resolution function as well as an additional Lorentzian contribution (the x parameter). As the sample is larger than the 0.8 x 0.8 $mm^2$ beam profile the Thompson-Cox-Hastings pseudo-Voight peak profile was convoluted with a top hat function with a fixed length found based on the $LaB_6$ line broadening standard.

*Two phase model ($Zn_4Sb_3$ + ZnSb)*

Here the $Zn_4Sb_3$ phase is refined alongside the ZnSb phase, primarily to obtain the weight fraction of ZnSb as the sample decomposes. The ZnSb phase is refined based on the structural model by Mozharivskyj *et al.* (ICSD 55403).[2] The refined parameters for the ZnSb phase were the scale factor, unit cell parameters and ADPs for Zn1 and Sb1. The peak profile was refined similarly to the $Zn_4Sb_3$ phase.

*Two phase model ($Zn_4Sb_3$ + Zn)*

Here the $Zn_4Sb_3$ phase is refined alongside the Zn phase, primarily to obtain the weight fraction of Zn as Zn migrates in the sample under operating conditions. The Zn phase is refined based on the structural model by Nuss *et al.* (ICSD 421015).[3] The refined parameters for the Zn phase were scale factor, unit cell parameters, ADP and peak profile similar to the $Zn_4Sb_3$ phase.

*Occupancy refinement ($Zn_4Sb_3$)*

This refinement model uses the three interstitial model to refine the occupancy of the main site and interstitial Zn sites. The ADPs correlate strongly with the site occupancy factors (SOFs), making co-refining of these challenging. Consequently, to refine the SOFs, the ADPs are fixed to the value obtained at each position after the maximum temperature is reached and the current turned on. This approach makes it possible to track relative changes in the SOFs as long as the temperature remains constant. The temperature is expected to remain relatively constant until the ZnSb phase front reaches the probed volume, whereby the temperature will rise due to increased Joule heating by the more resistive ZnSb phase. In the refinements SOF of the main site (Zn1) is refined while the SOF of three

interstitial sites (Zn2,Zn3,Zn4) are refined as equivalent. Additionally, the scale factor and unit cell parameters were refined.

2) Raw X-ray diffraction patterns for all samples

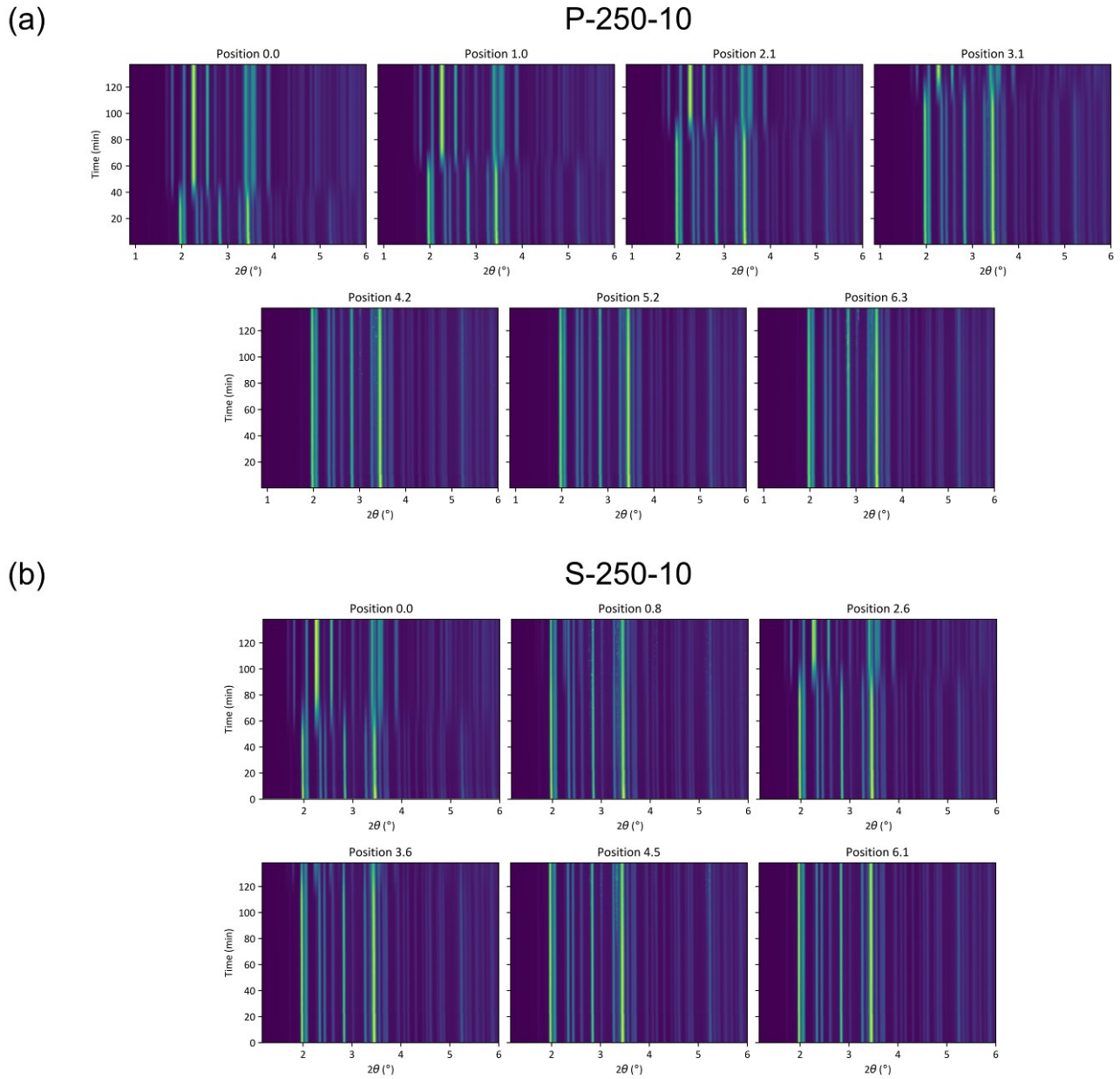


**Figure S1** Raw X-ray diffraction patterns for sample (a) P-250-10 and (b) S-250-10 at the different positions along the sample. Position numbers are distance from the first position, closest to the hot tower, given in mm.

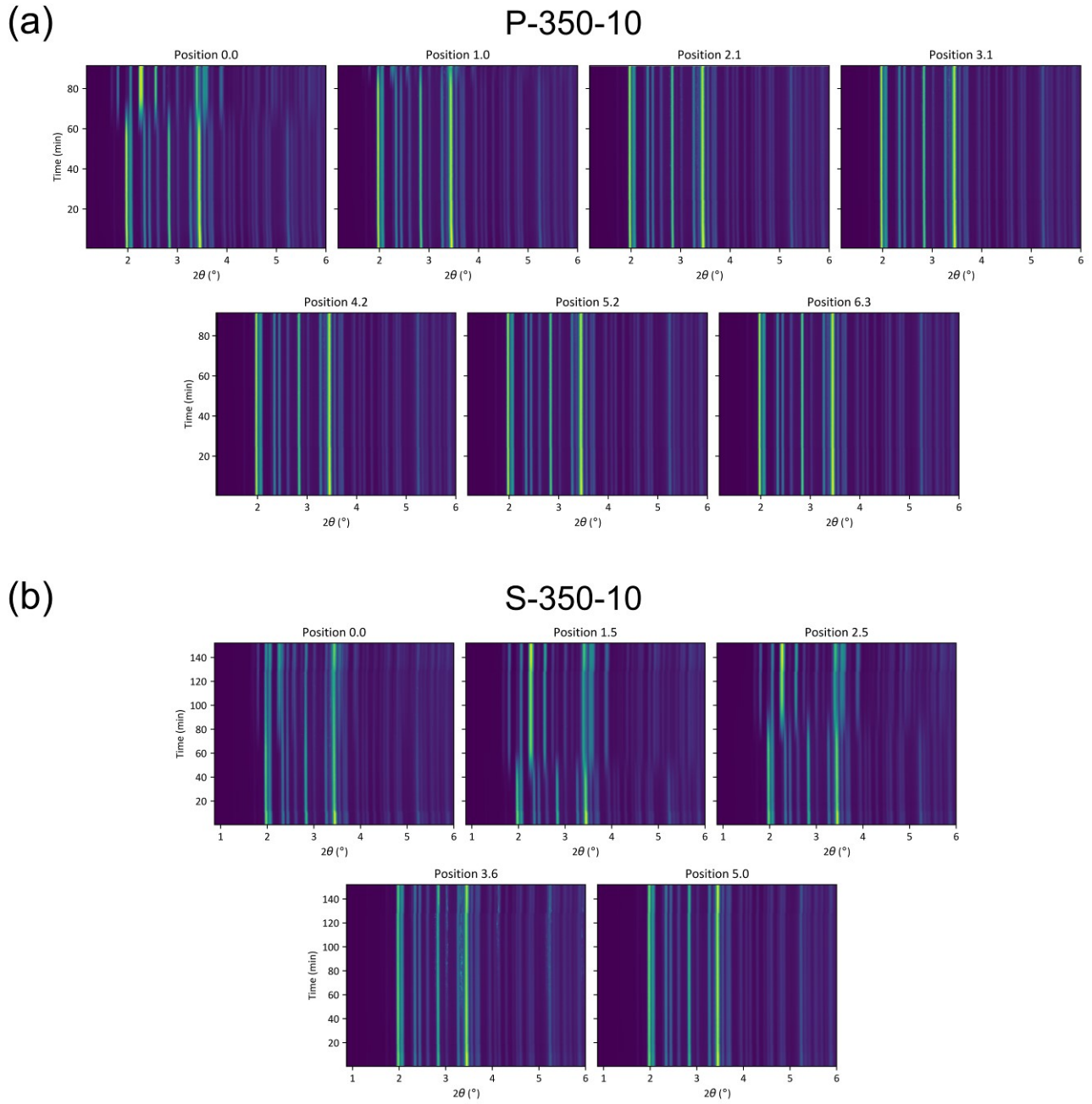


**Figure S2** Raw X-ray diffraction patterns for sample (a) P-350-10 and (b) S-350-10 at the different positions along the sample. Position numbers are distance from the first position, closest to the hot tower, given in mm.

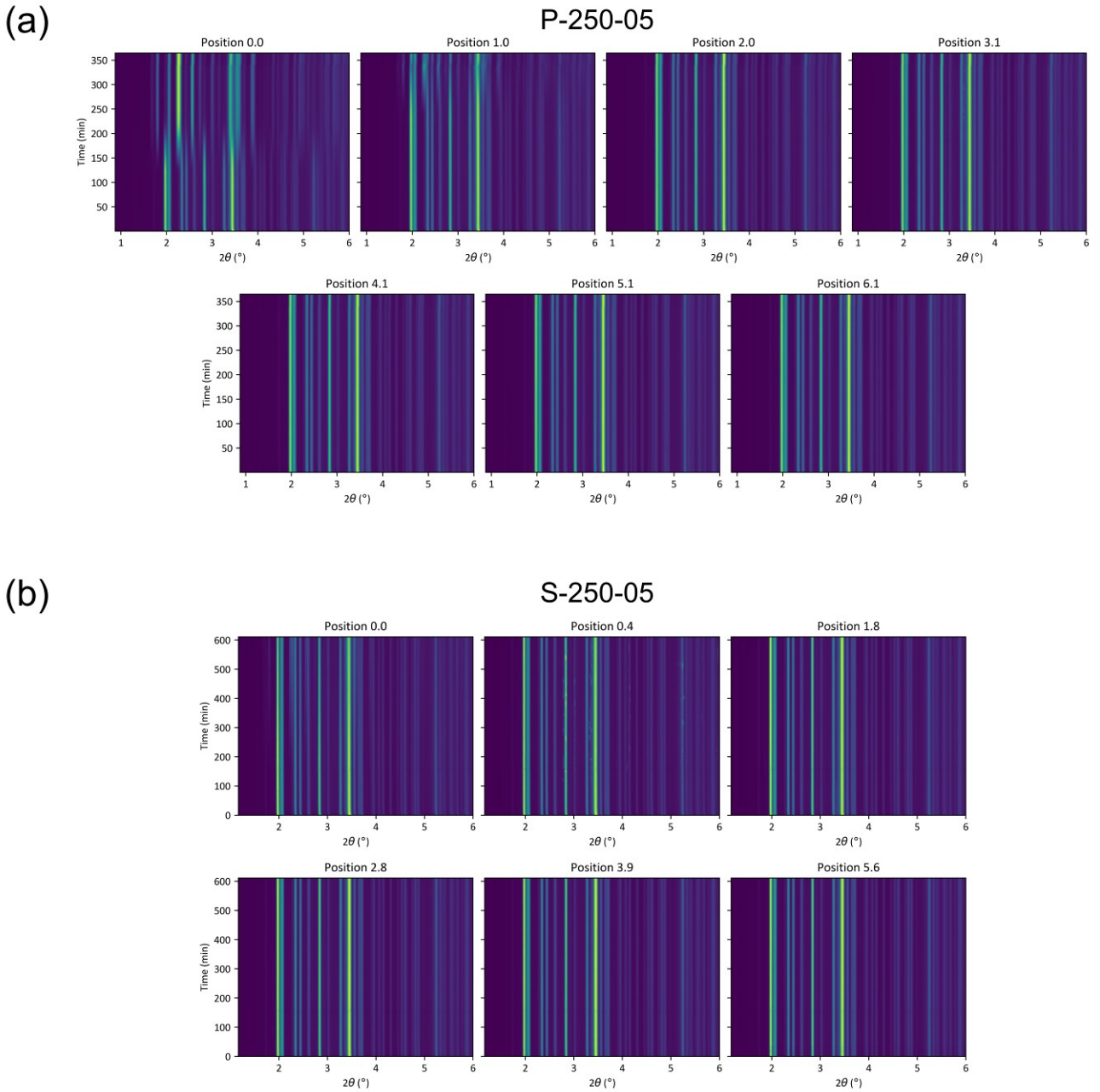


**Figure S3** Raw X-ray diffraction patterns for sample (a) P-250-05 and (b) S-250-05 at the different positions along the sample. Position numbers are distance from the first position, closest to the hot tower, given in mm.

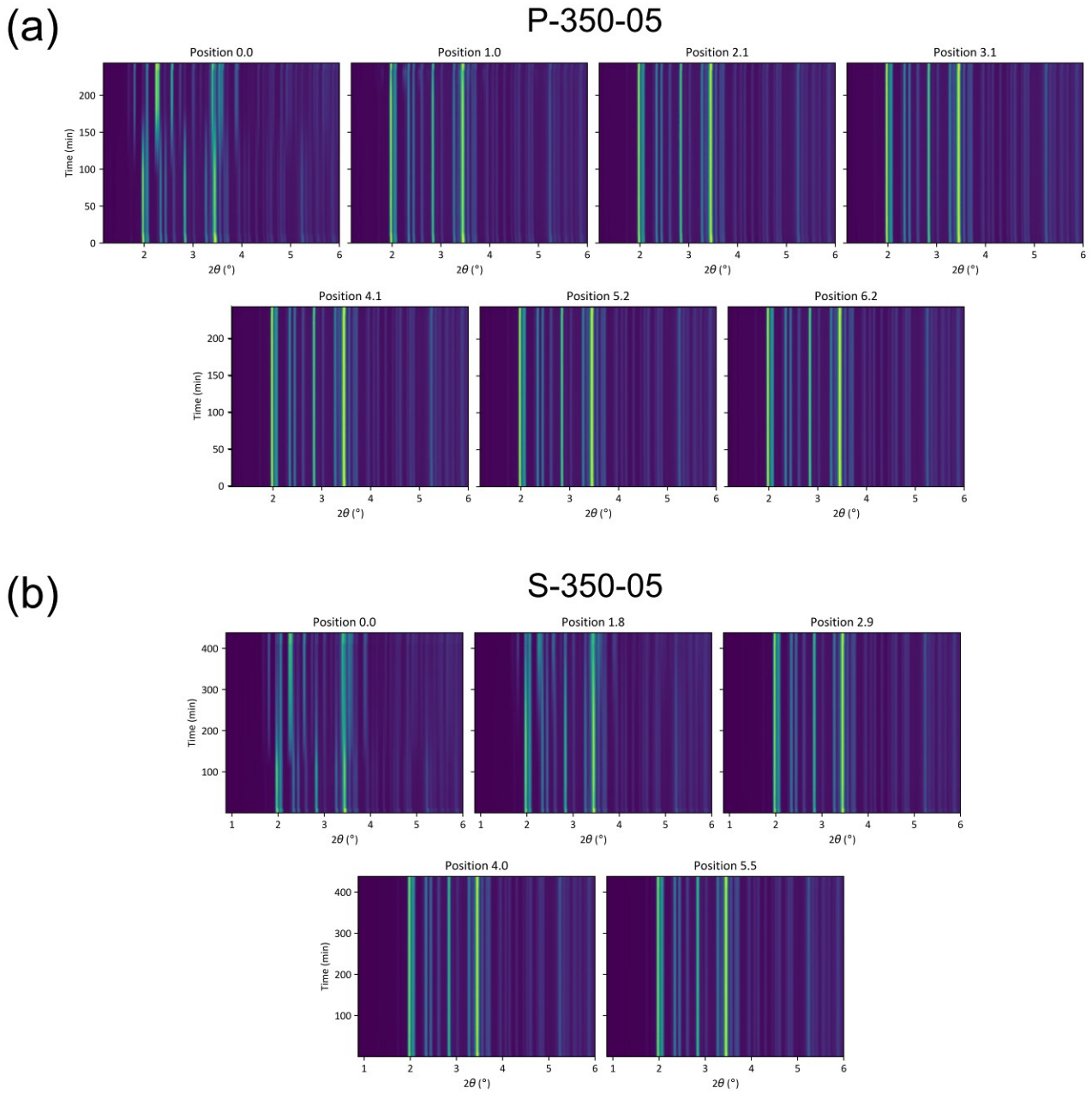


**Figure S4** Raw X-ray diffraction patterns for sample (a) P-350-05 and (b) S-350-05 at the different positions along the sample. Position numbers are distance from the first position, closest to the hot tower, given in mm.

3) Camera pictures of P- & S-250-10 samples

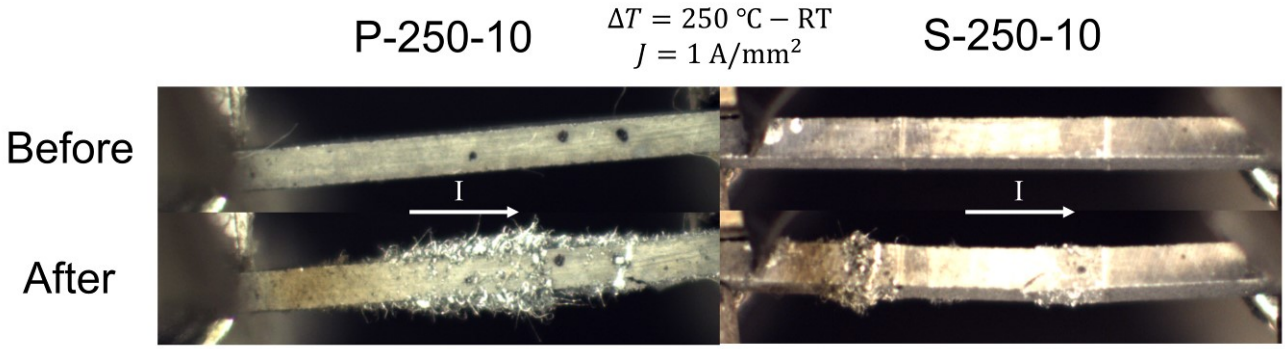


**Figure S5** Pictures of sample P-250-10 and S-250-10 before and after operando experiments. Zn whiskers grow out of the structure around the middle of the pure sample, while growing out right before the stainless steel ion-blocking interfaces in the segmented sample.

4) Refined weight fraction of ZnSb for datasets 350-05, 350-10, and 250-05

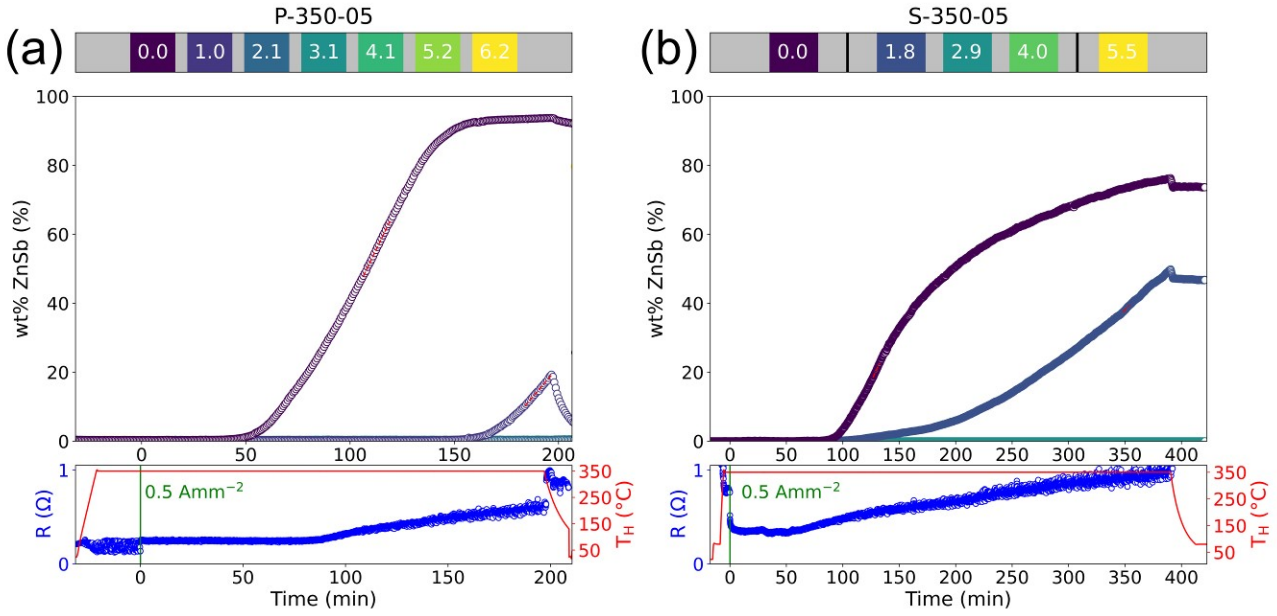


**Figure S6** Refined weight fractions of the ZnSb phase for (a) P-350-05 and (d) S-350-05. The measured 4 point resistance across the sample (blue) alongside the temperature profile (red) and onset of current (green) for (b) P-350-05 and (e) S-350-05. Sketch of the sample setup, with the measured positions along the sample is given for (c) P-350-05 and (f) S-350-05. The numbers indicate the distance from the first position (in mm) and the horizontal black lines in (f) indicate the position of the stainless steel interfaces.

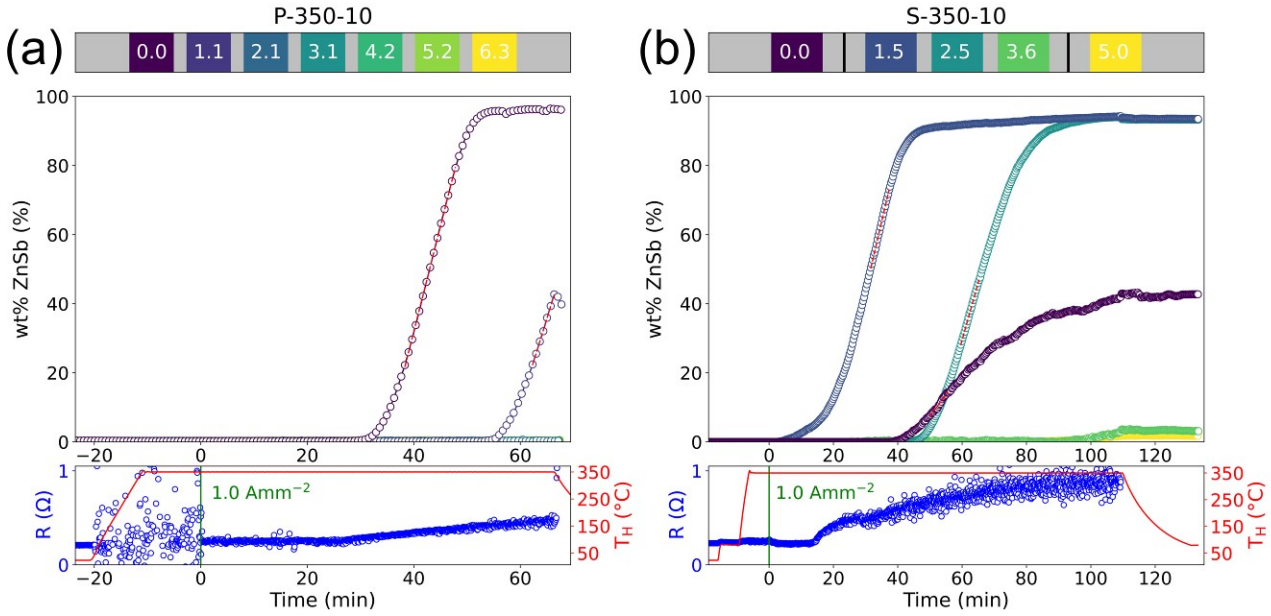


**Figure S7** Refined weight fractions of the ZnSb phase for (a) P-350-10 and (d) S-350-10. The measured 4 point resistance across the sample (blue) alongside the temperature profile (red) and onset of current (green) for (b) P-350-10 and (e) S-350-10. Sketch of the sample setup, with the measured positions along the sample is given for (c) P-350-10 and (f) S-350-10. The numbers indicate the distance from the first position (in mm) and the horizontal black lines in (f) indicate the position of the stainless steel interfaces.

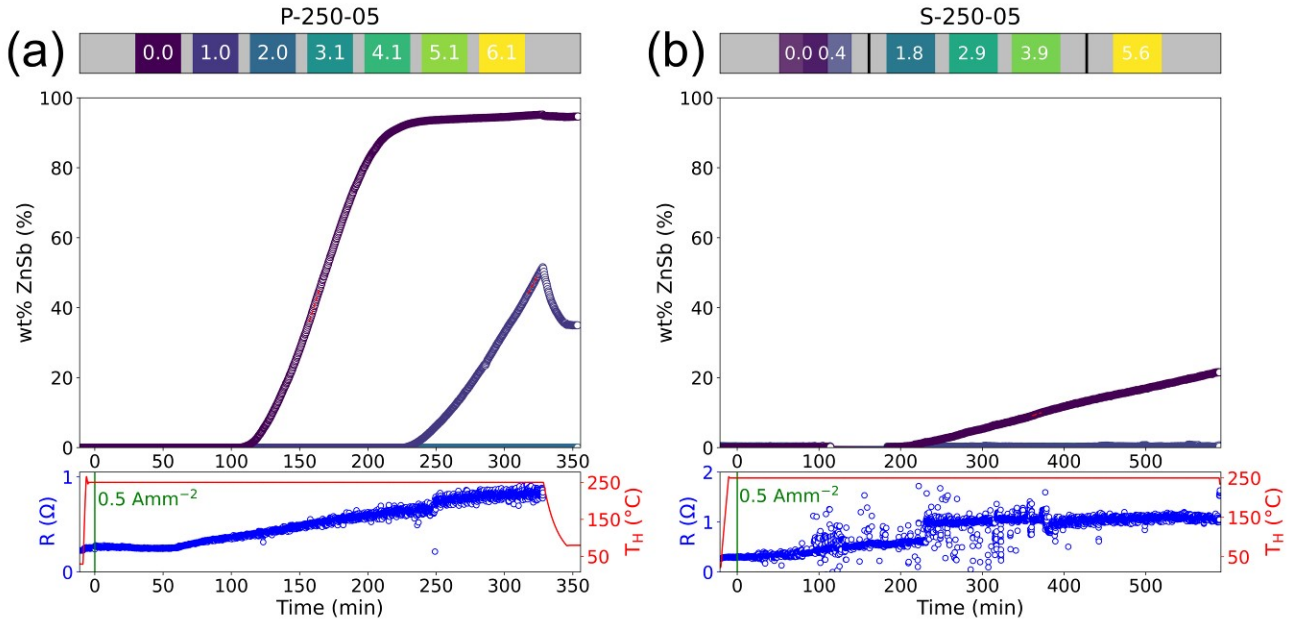


**Figure S8** Refined weight fractions of the ZnSb phase for (a) P-250-05 and (d) S-250-05. The measured 4 point resistance across the sample (blue) alongside the temperature profile (red) and onset of current (green) for (b) P-250-05 and (e) S-250-05. Sketch of the sample setup, with the measured positions along the sample is given for (c) P-250-05 and (f) S-250-05. The numbers indicate the distance from the first position (in mm) and the horizontal black lines in (f) indicate the position of the stainless steel interfaces.

5) Zoom of refined $Zn_4Sb_3$ weight fraction for P- & S-250-10

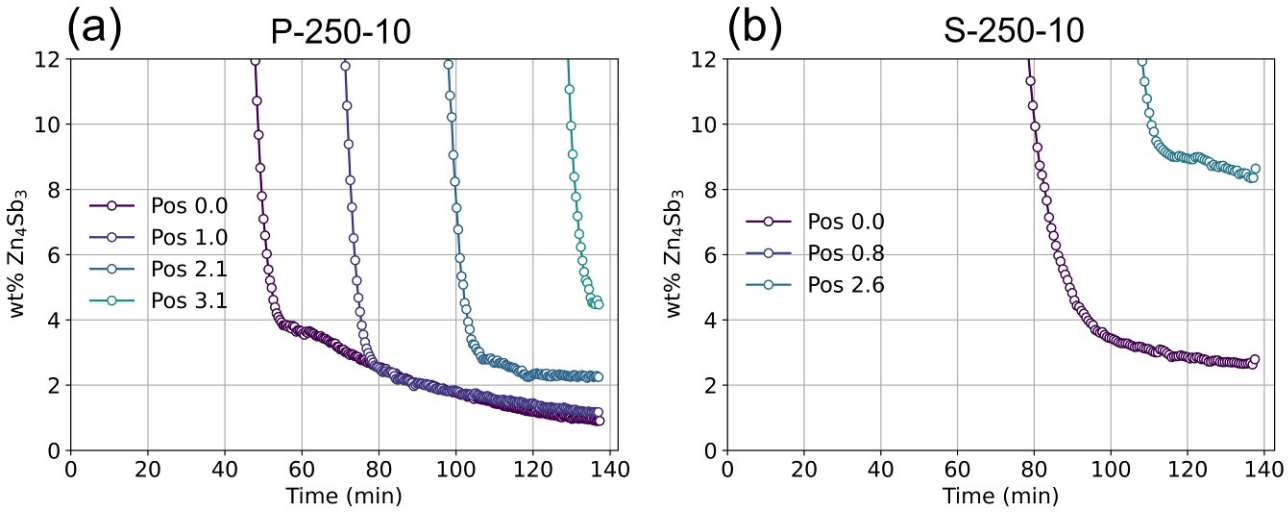


**Figure S9** Zoom on the refined weight fraction of the $Zn_4Sb_3$ phase as a function of time for sample (a) P-250-10 and (b) S-250-10. It is clear that a complete phase transition does not take place, and the weight fraction slopes only gradually decrease after a certain point for all positions.

6) Residual $Zn_4Sb_3$ phase in the X-ray diffraction patterns

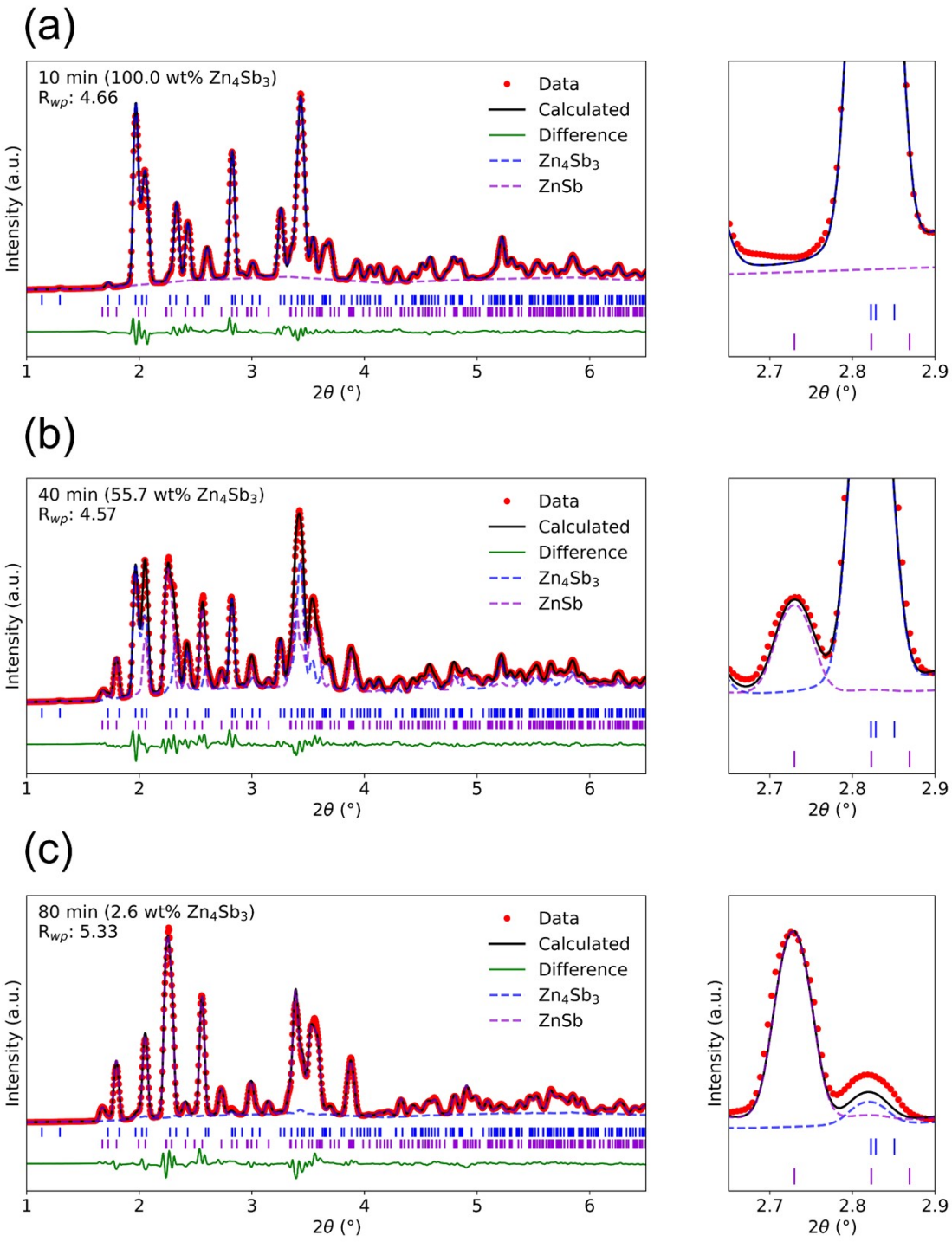


**Figure S10** Rietveld refinement on diffraction pattern for P-250-10 position 0.0 mm at time of (a) 10 min, (b) 40 min and (c) 80 min. Panel on the right in all subfigures is a zoom on a region (2.65-2.9 degrees) where the $Zn_4Sb_3$ phase is the main contributor to the peak at 2.82 degrees.

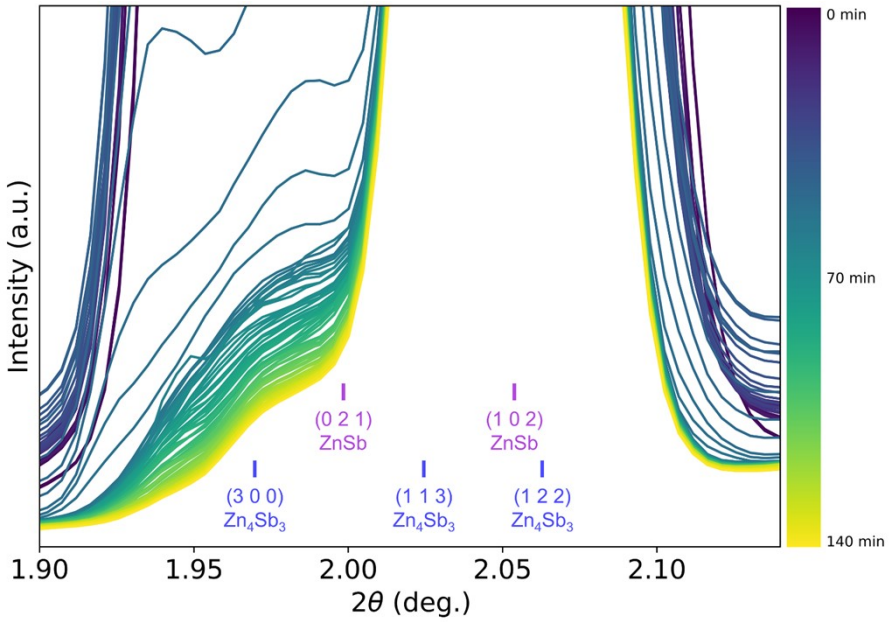


**Figure S11** Diffraction pattern of P-250-10 at position 0.0 mm in the 2θ region of 1.9°-2.15°, where separation of strong reflections between the $Zn_4Sb_3$ phase and the ZnSb phase can be separated. It is clear that the (3 0 0) reflection from the $Zn_4Sb_3$ gradually decrease long after the position has started to decompose (17 min), which indicate entrapment of some of the $Zn_4Sb_3$ phase in the hot end, that can only slowly decompose.

**Table S1** Refinement parameters for position 0.0 mm in the hot end of sample P-250-10 at 10 min, 40 min and 80 min (corresponding to the plots in Figure S10). *Values omitted, as the very small amount of $Zn_4Sb_3$ after 80 min results in the ADPs to refine to unphysical values with errors higher than their value.

| **Parameter** | **10 min** | **40 min** | **80 min** |
|---|---|---|---|
| $R_{wp}$ | 4.66 | 4.57 | 5.33 |
| $Zn_4Sb_3$ phase | | | |
| wt%($Zn_4Sb_3$) | 100(0) | 55.65(21) | 2.55(25) |
| $R_{bragg}$ | 2.08 | 1.91 | 3.69 |
| a, b [Å] | 12.28584(33) | 12.30178(57) | 12.2915(94) |
| c [Å] | 12.48884(60) | 12.5103(11) | 12.568(21) |
| $B_{iso}$ Zn1 [Å$^2$] | 3.455(66) | 3.72(11) | -* |
| $B_{iso}$ Zn2 [Å$^2$] | 4.62(58) | 6.80(122) | -* |
| $B_{iso}$ Sb1 [Å$^2$] | 1.796(39) | 1.906(72) | -* |
| $B_{iso}$ Sb2 [Å$^2$] | 1.609(47) | 1.982(88) | -* |
| ZnSb phase | | | |
| wt%(ZnSb) | 0 | 44.35(21) | 97.48(25) |
| $R_{bragg}$ | - | 2.35 | 3.06 |
| a [Å] | - | 6.24883(57) | 6.25225(34) |
| b [Å] | - | 7.77088(68) | 7.77443(41) |
| c [Å] | - | 8.10866(83) | 8.11242(46) |
| $B_{iso}$ Zn1 [Å$^2$] | - | 3.17(12) | 3.353(70) |
| $B_{iso}$ Sb1 [Å$^2$] | - | 1.433(49) | 1.546(30) |

7) Evolution of $R_{wp}$ for sample P-250-10

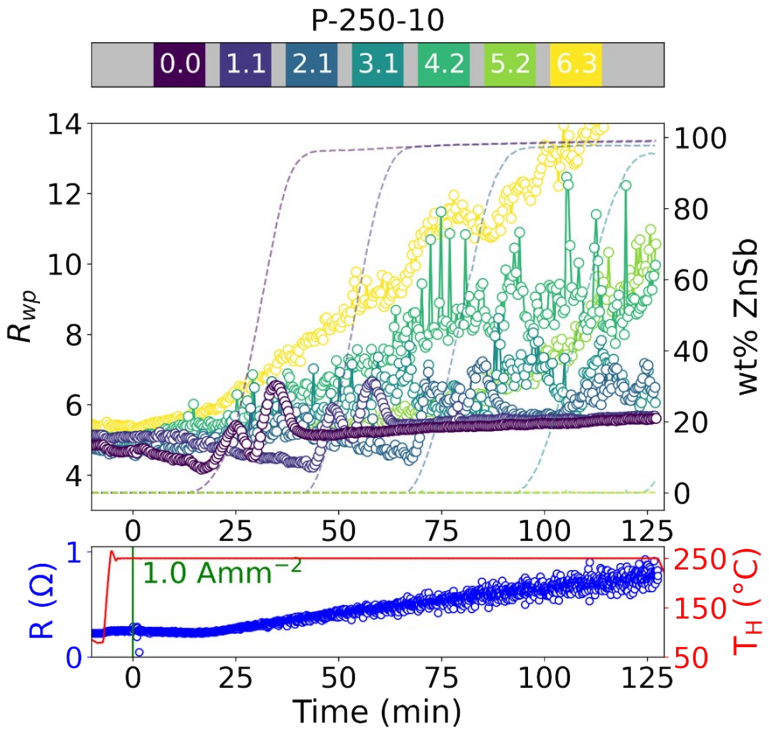


**Figure S12** $R_{wp}$ factors for sample P-250-10 as function of time (left y-axis) together with the refined weight fraction of ZnSb (dashed lines, right y-axis). The discrepancy increases during the phase transition and gets increasingly higher in the positions at the cold end where the un-refined Zn phase emerges.

8) Decomposition rates for datasets 250-05, 350-05 and 350-10

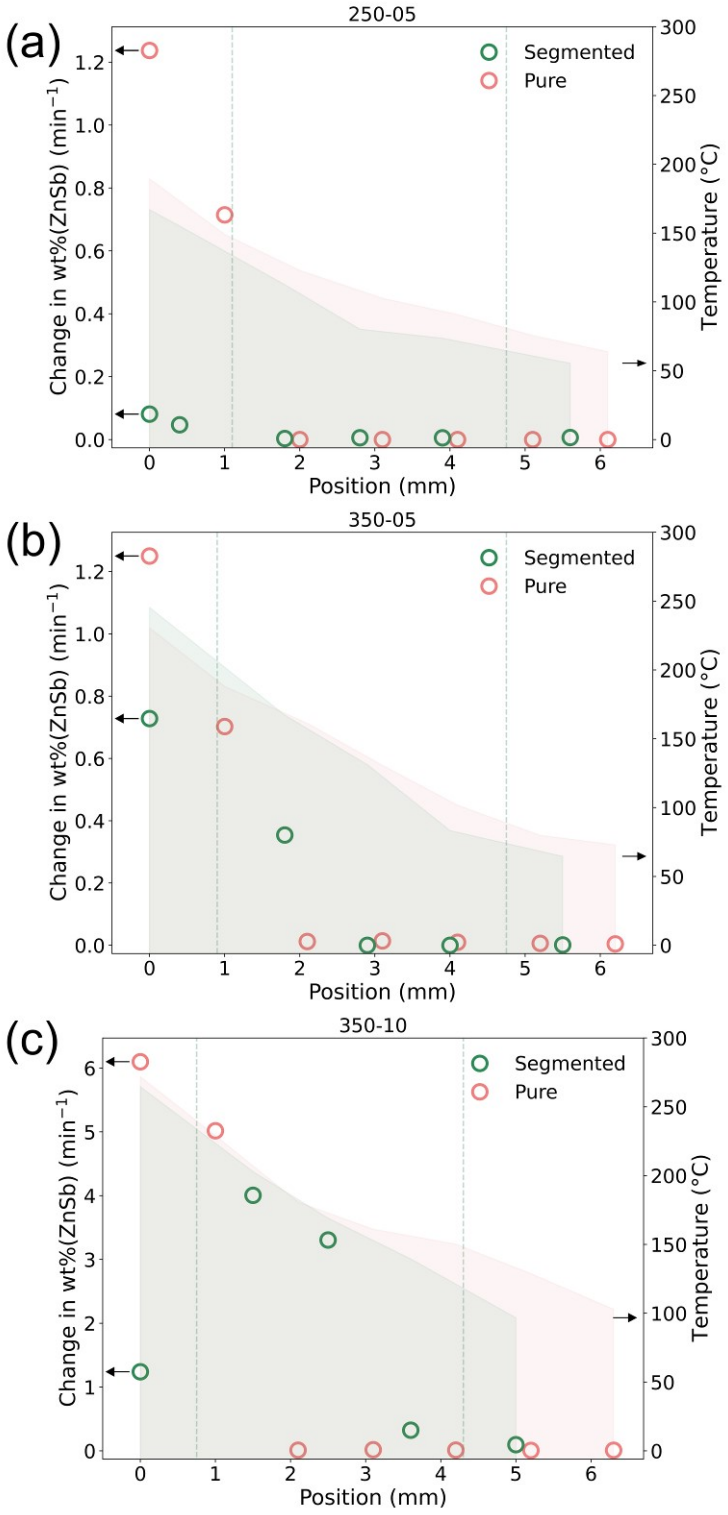


**Figure S13** Change in weight fractions (decomposition rates) for the different positions along the sample (left y-axis) accompanied with the estimated temperature from the unit cell expansion of

$Zn_4Sb_3$ (right y-axis) for (a) P-250-05 and S-250-05, (b) P-350-05 and S-350-05, and (c) P-350-10 and S-350-10.

9) Temperature gradient in P- & S-350-00

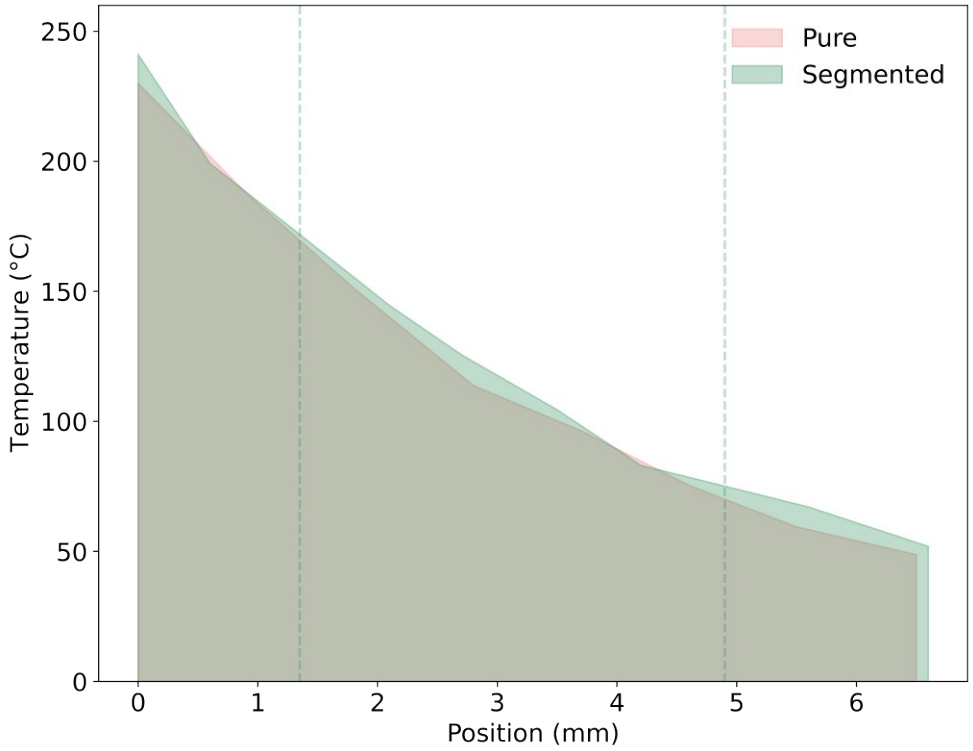


**Figure S14** Estimated temperature along sample P-350-00 and S-350-00, subjected to a temperature gradient of $\Delta T = 350\ ℃ - RT$ without any applied current.

10) Refined occupancy of main site Zn1 for all samples

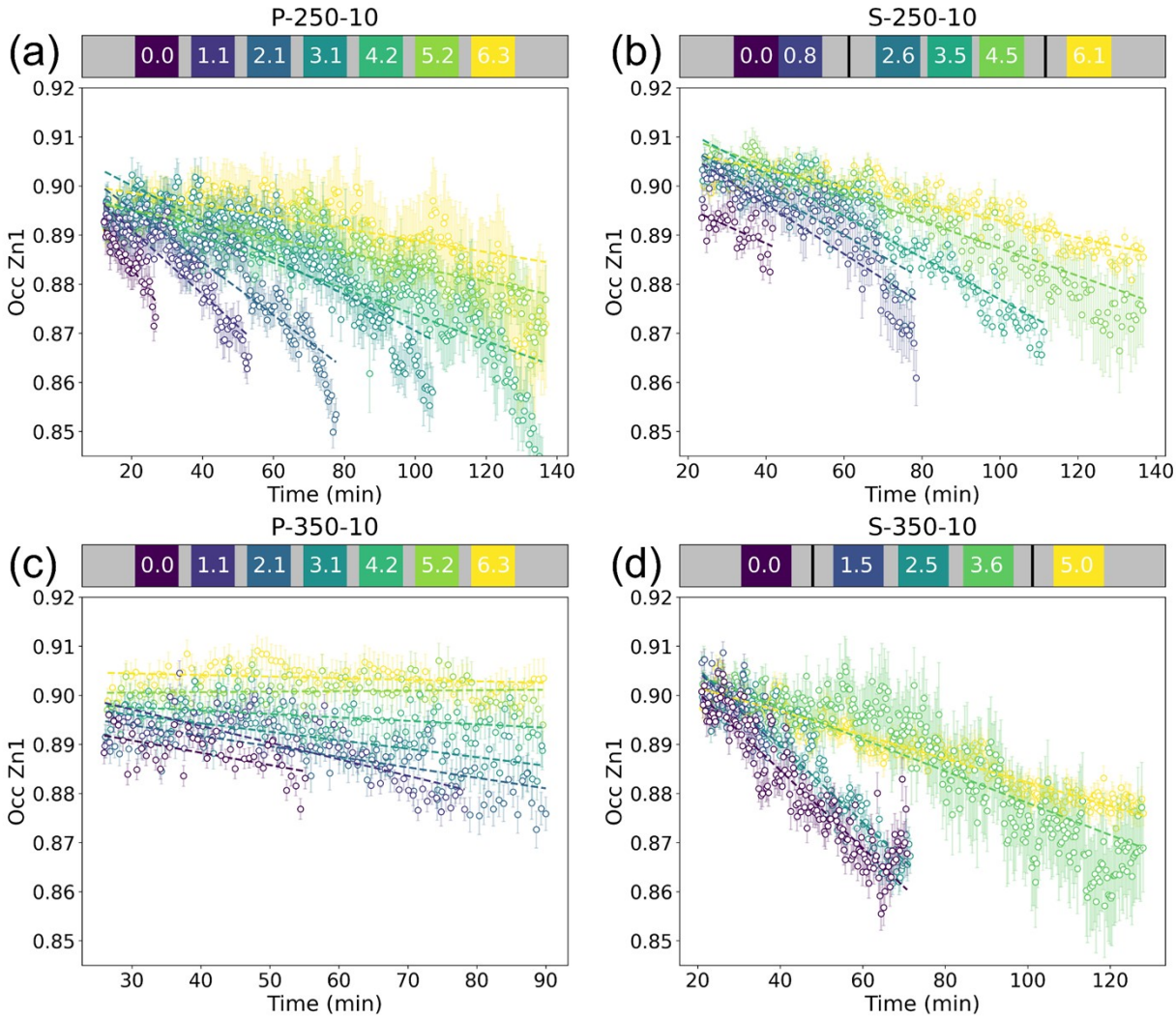


**Figure S15** Refined occupancies of the main site Zn1 site in $Zn_4Sb_3$ after the current is turned on and until the position decomposes for samples with current density of 1.0 $Amm^{-2}$, a) P-250-10, b) S-250-10, c) P-350-10, and d) S-350-10. The dashed lines show the linear fit to the slope in occupancy.

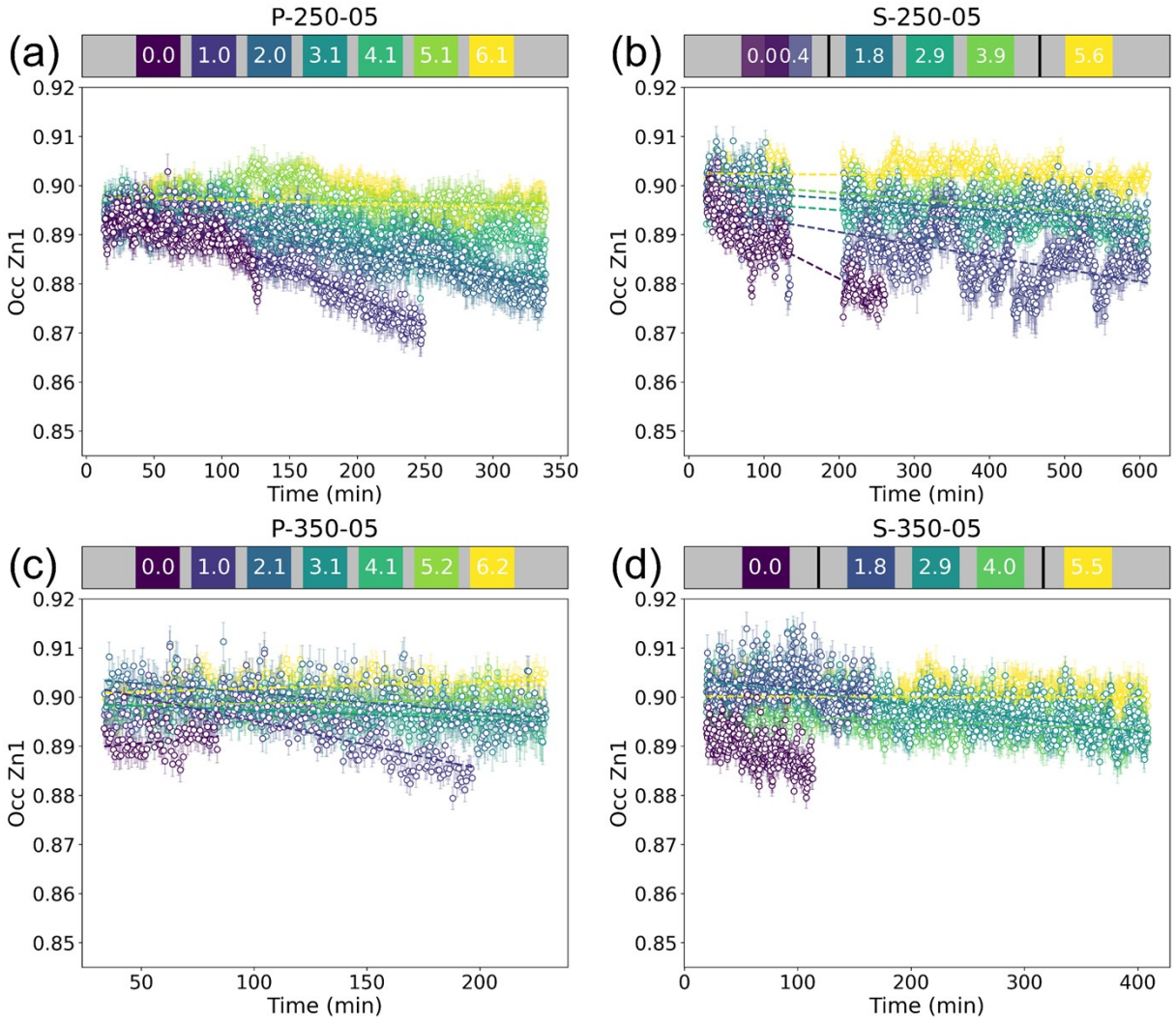


**Figure S16** Refined occupancies of the main site Zn1 site in $Zn_4Sb_3$ after the current is turned on and until the position decomposes for samples with current density of 0.5 $Amm^{-2}$, a) P-250-05, b) S-250-05, c) P-350-05, and d) S-350-05. The dashed lines show the linear fit to the slope in occupancy.

11) Refined total Zn content for all samples

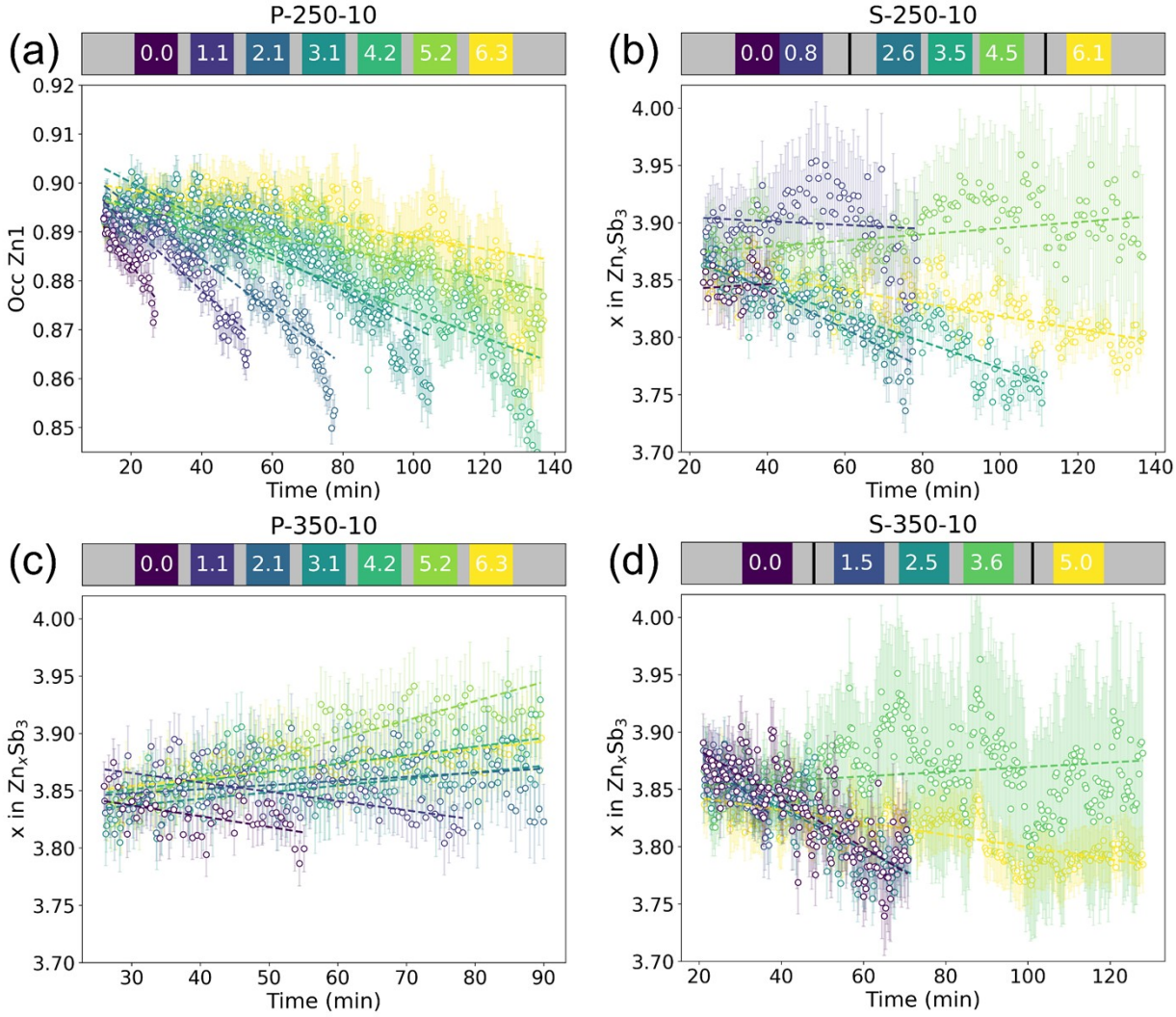


**Figure S17** Combination of the refined main site Zn1 and interstitial site Zn2 converted to the total Zn content *x* in $Zn_xSb_3$ using the multiplicities of the specific sites in the crystal structure, plotted for samples with current density of 1.0 $Amm^{-2}$, a) P-250-10, b) S-250-10, c) P-350-10, and d) S-350-10. The dashed lines show the linear fit to the slope of change in total Zn content.

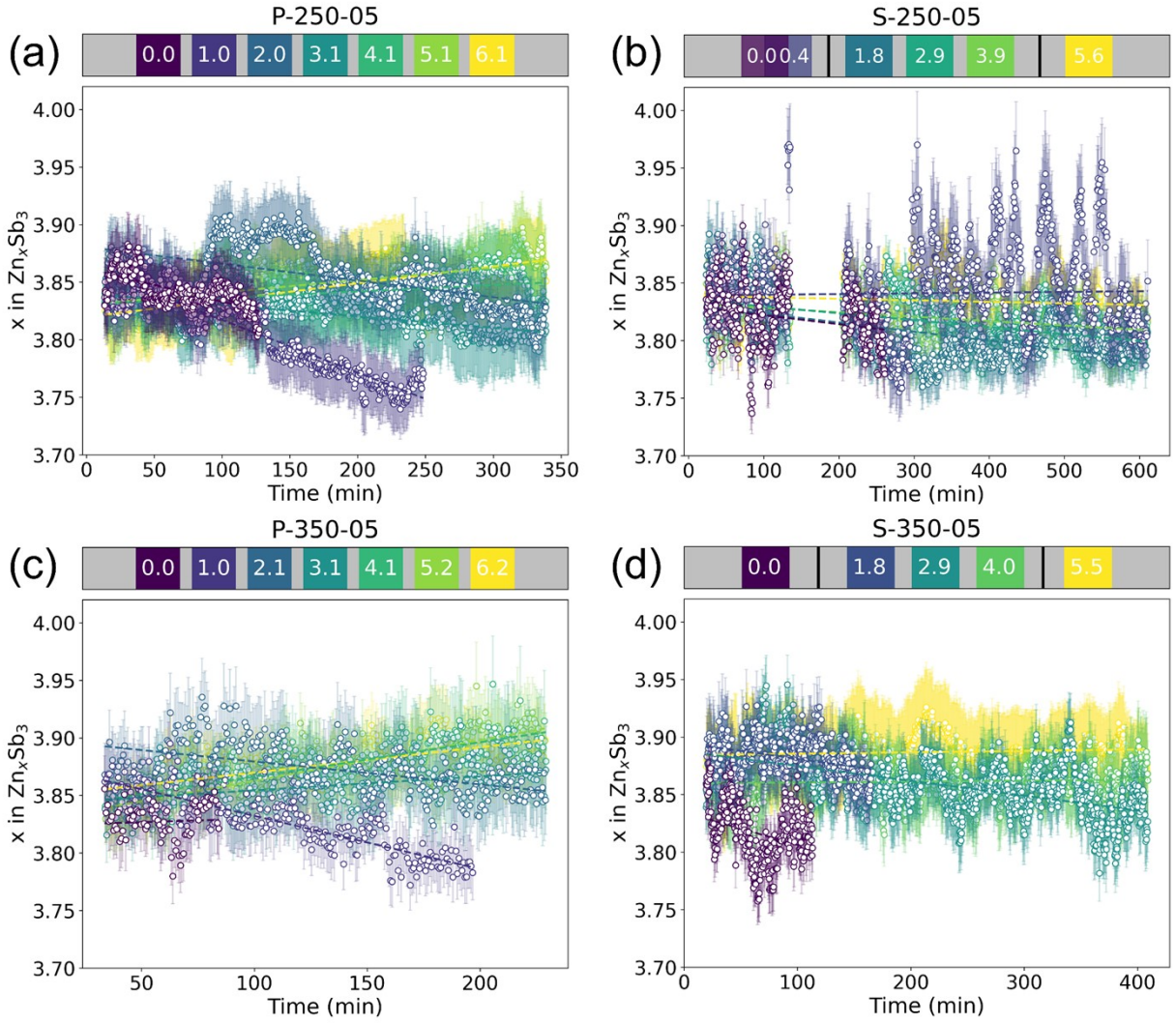


**Figure S18** Combination of the refined main site Zn1 and interstitial site Zn2 converted to the total Zn content *x* in $Zn_xSb_3$ using the multiplicities of the specific sites in the crystal structure, plotted for samples with current density of 0.5 $Amm^{-2}$, a) P-250-05, b) S-250-05, c) P-350-05, and d) S-350-05. The dashed lines show the linear fit to the slope of change in total Zn content.

## 12) Zn migration rates for datasets 250-05, 350-05, and 350-10

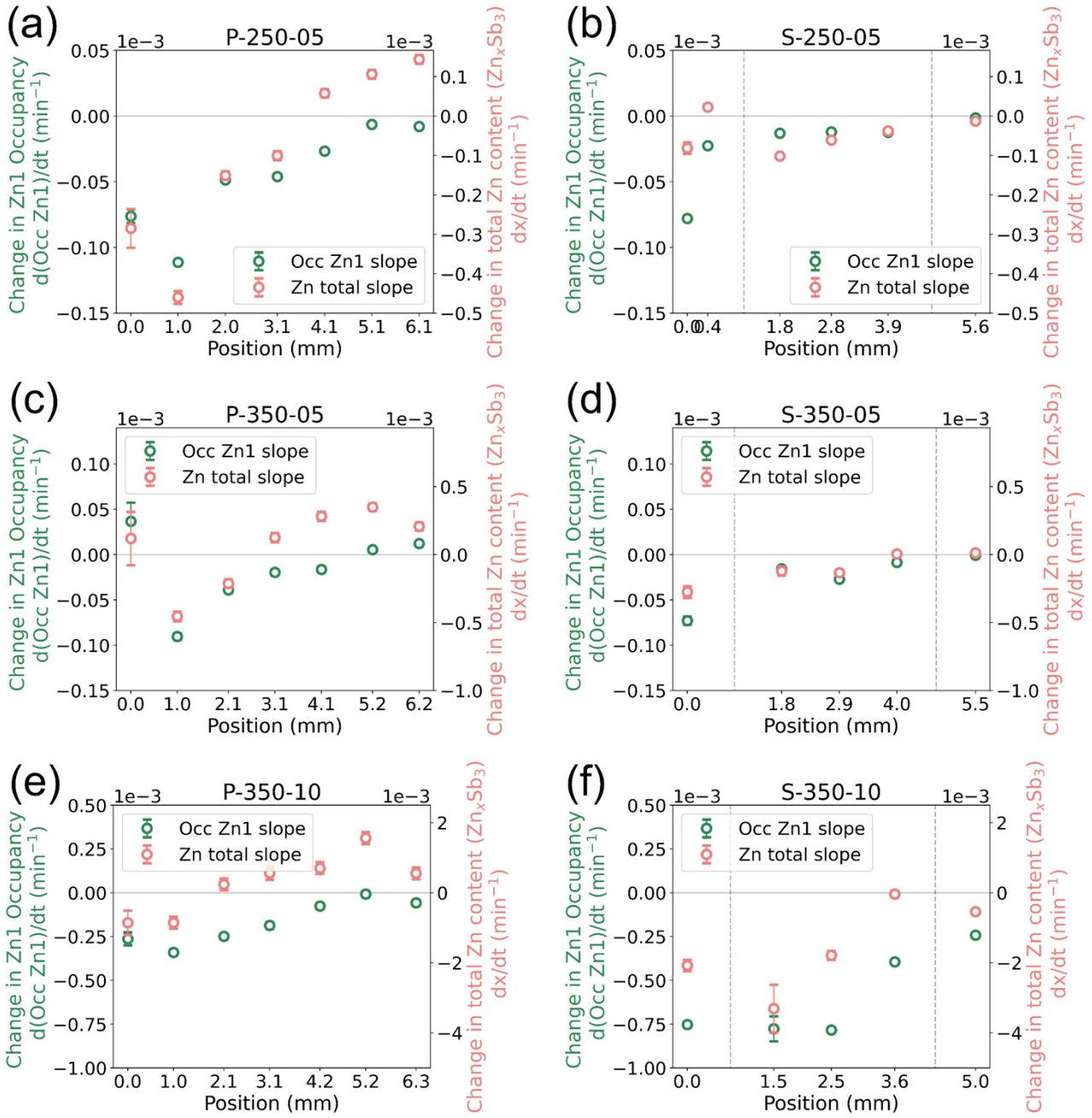


**Figure S19** Value of the change with respect to time of main site Zn1 occupancy (green) and total Zn content (red) at the various positions along the samples for(a) P-250-05, (b) S-250-05, (c) P-350-05, (d) S-350-05, (e) P-350-10, and (f) S-350-10. .

13) Zn peaks in raw diffraction patterns for S-250-10

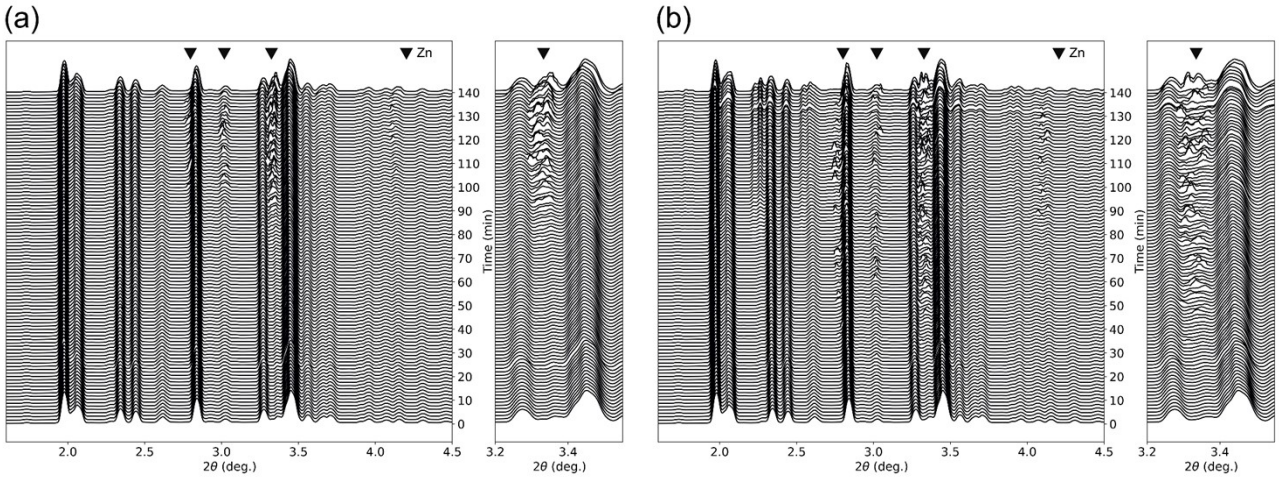


**Figure S20** Raw diffraction patterns for sample S-250-10 from position (a) 0.8 mm and (b) 4.5 mm, that are both right before an ion blocking interface. Growth of Zn is clear at these positions which sediments the ability of the interfaces to block the migrating Zn ions. The growth of Zn appears as needle-shaped whiskers on the surface, which results in spotty and irregular diffraction peaks.

14) Refined Zn weight fraction for sample P- & S-250-10

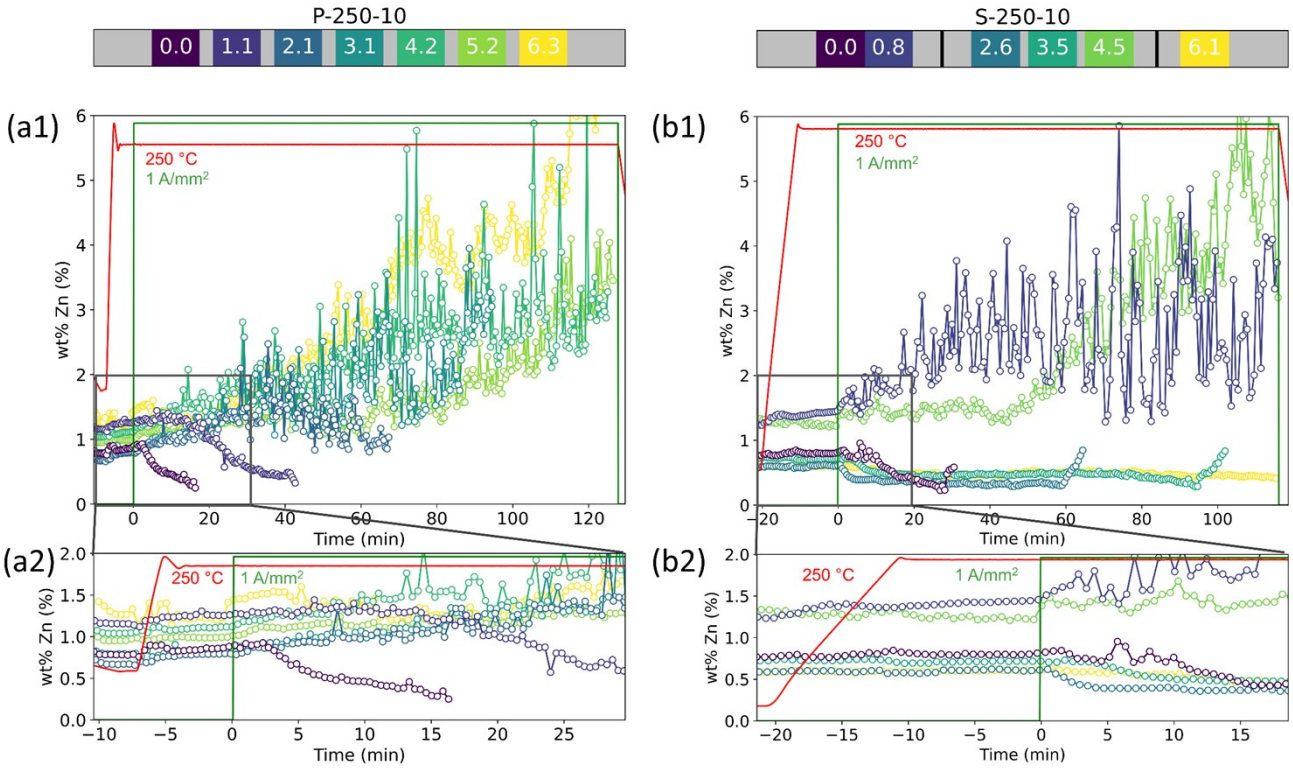


**Figure S21** Refined weight fraction of Zn at all positions for sample (a1) P-250-10 and (b1) S-250-10. The Zn whiskers gives rise to irregular diffraction peaks that makes a reliable Rietveld refinement difficult, which results in the large oscillations of the weight fractions. The plot is cut at each position when it decomposes, as the increasing ZnSb phase is erroneously ascribed to Zn. Zoom on the first region (black square) when the current is turned on for (a2) P-250-10 and (b2) S-250-10. The immediate decrease of the Zn weight fraction at positions 0.0 and 1.0 for P-250-10 and 0.0, 2.6, 3.6, and 4.5 for S-250-10 indicates the migration of Zn as the current is turned on in sample S-250-10.

15) SEM images of sample S-350-10

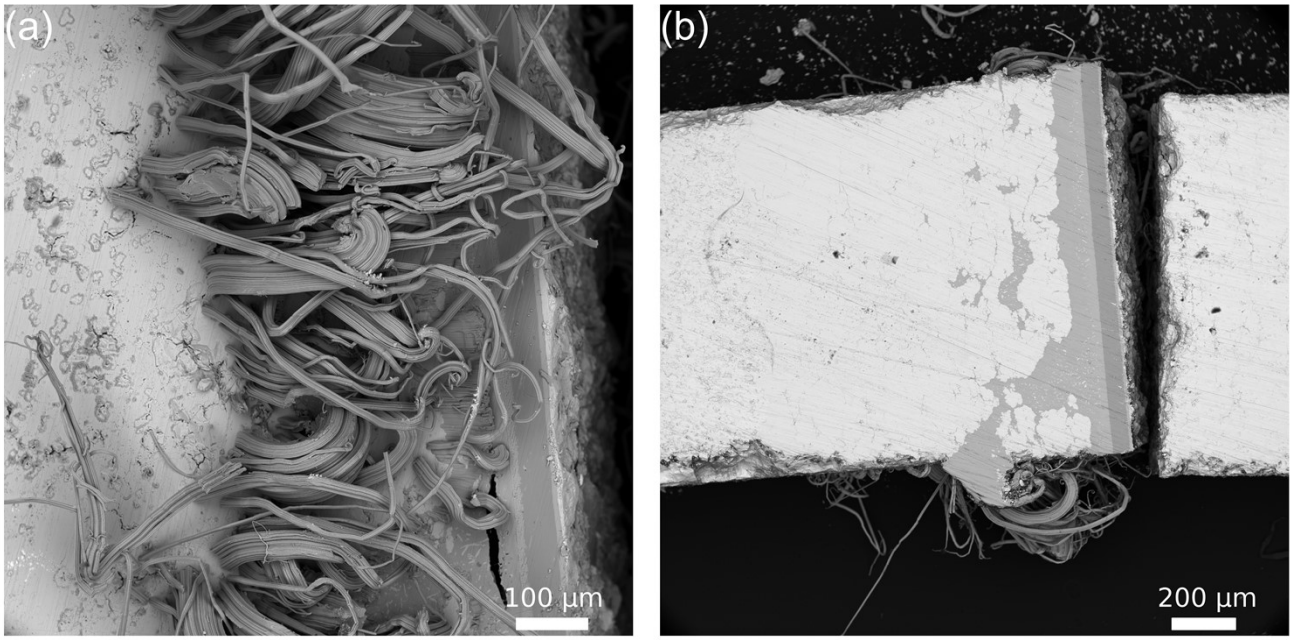


**Figure S22** Sample S-350-10 at the first interface (a) before polishing and (b) after polishing.

16) SEM images of the Zn phase front

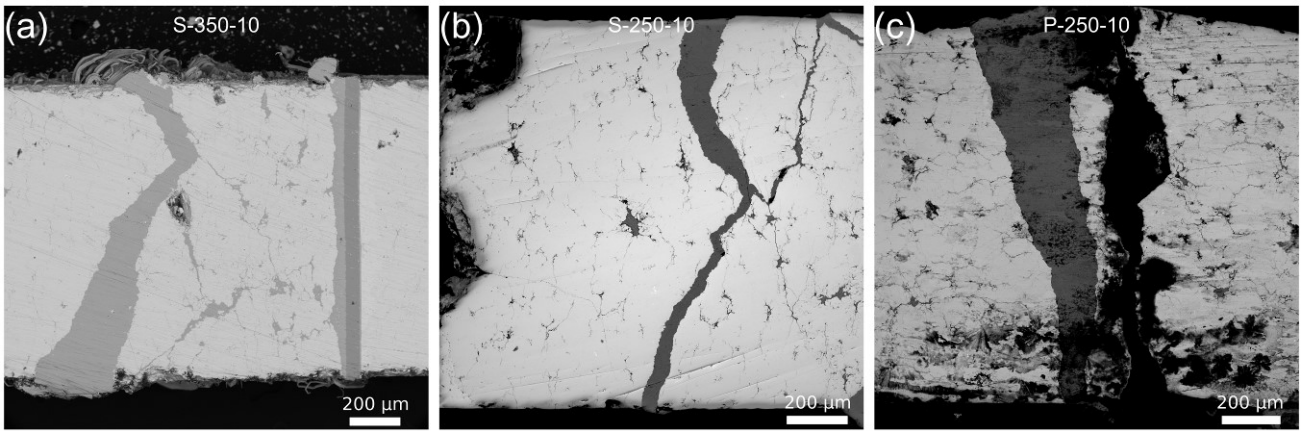


**Figure S23** SEM pictures (backscatter electrons) of the Zn phase front in (a) S-350-10 segment 2, (b) S-250-10 segment 2, and (c) P-250-10.

17) SEM images of the ZnSb phase front

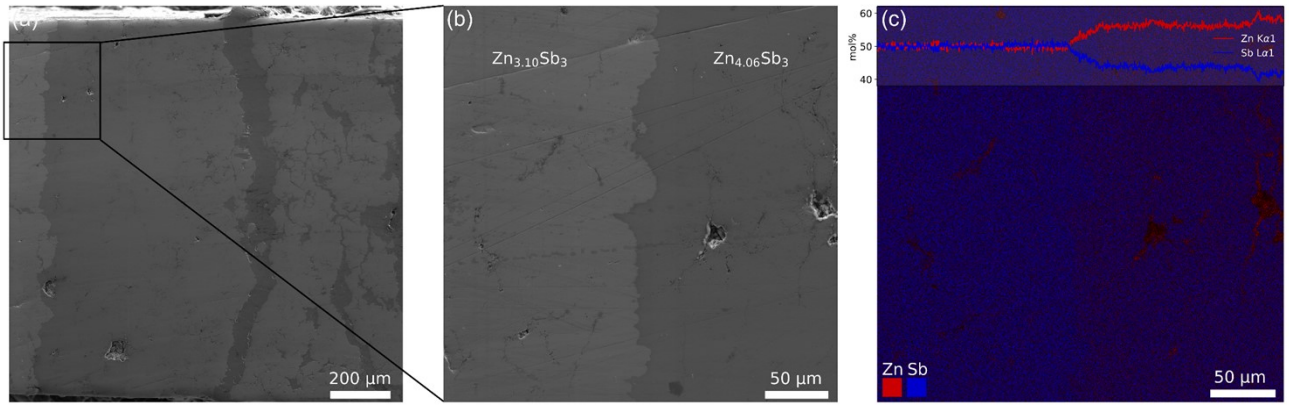


**Figure S24** (a) SEM image (secondary electrons) of S-250-10 where the phase front of ZnSb is clearly distinguished. (b) Zoomed region at the ZnSb-$Zn_4Sb_3$ phase boundary. Inserted compositions are average compositions in the two regions. (b) EDX map and line scan across the ZnSb-$Zn_4Sb_3$ phase boundary where the Zn and Sb ratio evidently goes from 1:1 to 4:3.

18) SEM of second interface in sample S-250-10

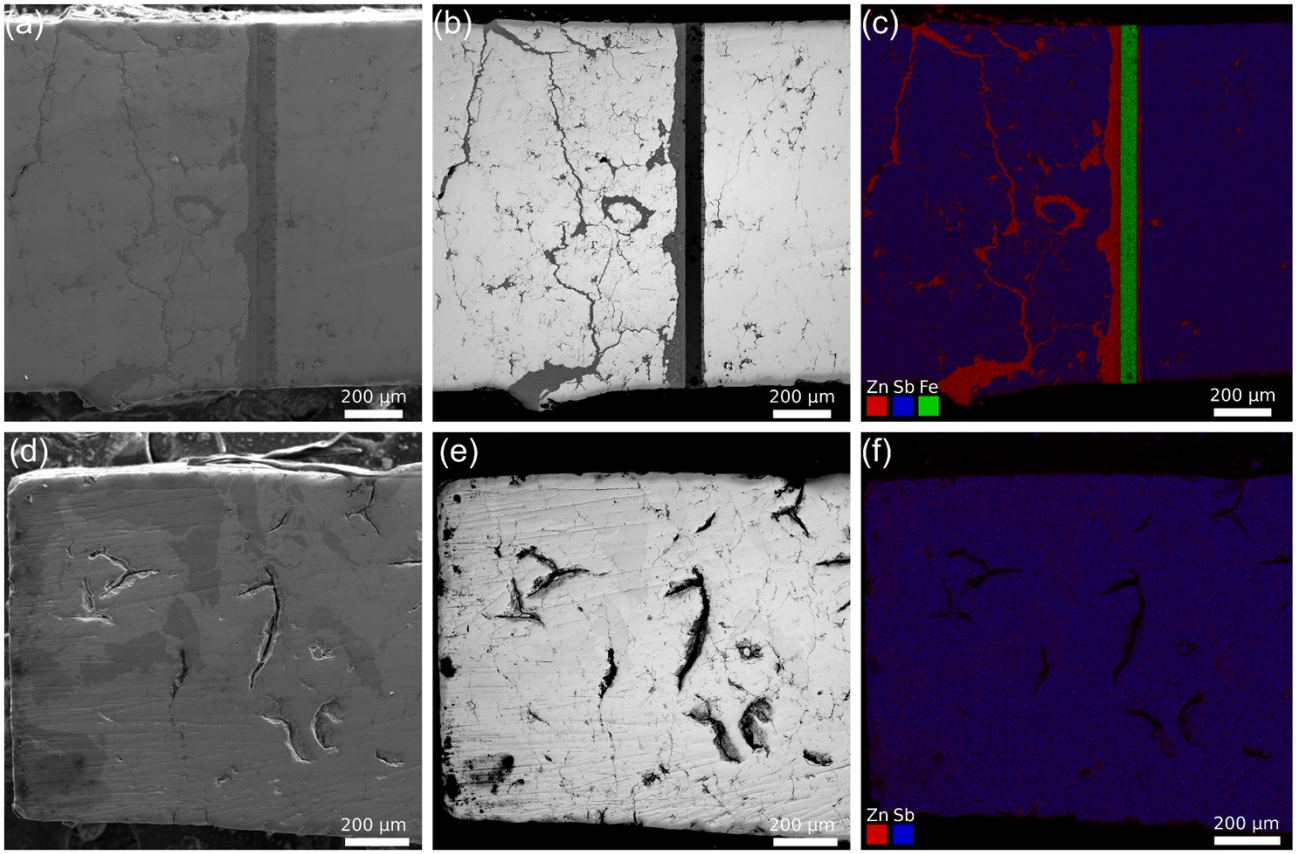


**Figure S25** SEM images of the second interface of sample S-250-10 taken with (a) secondary electrons (E-T detector), (b) backscattered electrons (BSE-4Q detector), and (c) EDX detector. SEM images of the left of the first segment (hot end) of sample S-250-10 taken with (a) secondary electrons (E-T detector), (b) backscattered electrons (BSE-4Q detector), and (c) EDX detector.

## 19) References


1 G. J. Snyder, M. Christensen, E. Nishibori, T. Caillat and B. B. Iversen, *Nat. Mater.*, 2004, **3**, 458–463.

2 Y. Mozharivskyj, A. O. Pecharsky, S. Bud'ko and G. J. Miller, *Chem. Mater.*, 2004, **16**, 1580–1589.

3 J. Nuss, U. Wedig, A. Kirfel and M. Jansen, *Zeitschrift fur Anorg. und Allg. Chemie*, 2010, **636**, 309–313.